JCI The Journal of Clinical Investigation

CD8$^+$ T cells target cerebrovasculature in children with cerebral malaria

Brittany A. Riggle, … , Dorian B. McGavern, Susan K. Pierce

J Clin Invest. 2020. https://doi.org/10.1172/JCI133474.

Clinical Research and Public Health | Infectious disease | Neuroscience

Cerebral malaria (CM) accounts for nearly 400,000 deaths annually in African children. Current dogma suggests that CM results from infected RBC (iRBC) sequestration in the brain microvasculature and resulting sequelae. Therapies targeting these events have been unsuccessful; findings in experimental models suggest that CD8$^+$ T cells drive disease pathogenesis. However, these data have largely been ignored because corroborating evidence in humans is lacking. This work fills a critical gap in our understanding of CM pathogenesis that is impeding development of therapeutics.

Using multiplex immunohistochemistry, we characterized cerebrovascular immune cells in brain sections from 34 children who died from CM or other causes. Children were grouped by clinical diagnosis (CM$^+$ or CM$^-$), iRBC sequestration (Seq^{hi}, Seq^{lo}, Seq^0) and HIV status (HIV$^+$ or HIV$^-$).

We identified effector CD3$^+$CD8$^+$ T cells engaged on the cerebrovasculature in 69% of CM$^+$ HIV$^-$ children. The number of intravascular CD3$^+$CD8$^+$ T cells was influenced by CM status (CM$^+$ > CM$^-$, $P = 0.004$) and sequestration level (Seq^{hi} > Seq^{lo}, $P = 0.010$). HIV coinfection significantly increased T cell numbers ($P = 0.017$) and shifted cells from an intravascular ($P = 0.004$) to perivascular ($P < 0.0001$) distribution.

Within the studied cohort, CM is associated with cerebrovascular engagement of CD3$^+$CD8$^+$ T cells, which is exacerbated by HIV coinfection. Thus, CD3$^+$CD8$^+$ T cells are highly promising targets for […]

CD8+ T cells target cerebrovasculature in children with cerebral malaria

Brittany A. Riggle,[1] Monica Manglani,[2,3] Dragan Maric,[4] Kory R. Johnson,[5] Myoung-Hwa Lee,[6] Osorio Lopes Abath Neto,[7] Terrie E. Taylor,[8,9] Karl B. Seydel,[8,9] Avindra Nath,[6] Louis H. Miller,[10] Dorian B. McGavern,[2] and Susan K. Pierce[1]

[1]Laboratory of Immunogenetics, National Institute of Allergy and Infectious Diseases (NIAID), NIH, Rockville, Maryland, USA. [2]Viral Immunology and Intravital Imaging Section, National Institute of Neurological Disorders and Stroke (NINDS), NIH, Bethesda, Maryland, USA. [3]Medicial Scientist Training Program, Pennsylvania State College of Medicine, Hershey, Pennsylvania, USA. [4]Flow and Imaging Cytometry Core Facility, [5]Information Technology Program, Division of Intramural Research, and [6]Section of Infections of the Nervous System, National Institute of Neurological Disorders and Stroke, and [7]Laboratory of Pathology, National Cancer Institute, NIH, Bethesda, Maryland, USA. [8]Department of Osteopathic Medical Specialties, College of Osteopathic Medicine, Michigan State University, East Lansing, Michigan, USA. [9]Blantyre Malaria Project, University of Malawi College of Medicine, Blantyre, Malawi, Africa. [10]Laboratory of Malaria Vector Research, National Institute of Allergy and Infectious Diseases, NIH, Rockville, Maryland, USA.

BACKGROUND. Cerebral malaria (CM) accounts for nearly 400,000 deaths annually in African children. Current dogma suggests that CM results from infected RBC (iRBC) sequestration in the brain microvasculature and resulting sequelae. Therapies targeting these events have been unsuccessful; findings in experimental models suggest that CD8+ T cells drive disease pathogenesis. However, these data have largely been ignored because corroborating evidence in humans is lacking. This work fills a critical gap in our understanding of CM pathogenesis that is impeding development of therapeutics.

METHODS. Using multiplex immunohistochemistry, we characterized cerebrovascular immune cells in brain sections from 34 children who died from CM or other causes. Children were grouped by clinical diagnosis (CM^+ or CM^-), iRBC sequestration (Seq^{hi}, Seq^{lo}, Seq^0) and HIV status (HIV^+ or HIV^-).

RESULTS. We identified effector $CD3^+CD8^+$ T cells engaged on the cerebrovasculature in 69% of CM^+ HIV^- children. The number of intravascular $CD3^+CD8^+$ T cells was influenced by CM status ($CM^+ > CM^-$, $P = 0.004$) and sequestration level ($Seq^{hi} > Seq^{lo}$, $P = 0.010$). HIV coinfection significantly increased T cell numbers ($P = 0.017$) and shifted cells from an intravascular ($P = 0.004$) to perivascular ($P < 0.0001$) distribution.

CONCLUSION. Within the studied cohort, CM is associated with cerebrovascular engagement of $CD3^+CD8^+$ T cells, which is exacerbated by HIV coinfection. Thus, $CD3^+CD8^+$ T cells are highly promising targets for CM adjunctive therapy, opening new avenues for the treatment of this deadly disease.

FUNDING. This research was supported by the Intramural Research Program of the National Institutes of Health.

Introduction

Plasmodium falciparum malaria is a potentially fatal infectious disease caused by mosquito-transmitted parasites. Last year *P. falciparum* infections caused over 219 million cases of malaria and 435,000 deaths, the vast majority of which were young African children (1). The deadliest complication of infection is cerebral malaria (CM), causing greater than 90% of malarial fatalities. The mortality for CM is high, estimated to be 15%–25%, despite treatment with highly effective anti-malarial drugs (2). Tragically, many children who survive CM suffer from life-long sequelae, including debilitating cognitive, hearing, and vision impairments (3). Critically, we have no effective vaccines to protect children against malaria nor are there adjunctive CM therapies to combine with rapid-acting antimalarial drugs. Given the global burden of severe malaria, the development of a CM therapy is a public health and humanitarian priority.

The current standard of care for children with CM is artemisinin-based intravenous antimalarial therapy, clinical monitoring, and treatment of any secondary complications (e.g., seizures, anemia). Despite intensive investigation into the underlying pathophysiology of CM, at present our knowledge of the cellular and molecular mechanisms that underlie disease pathology is incomplete. Taylor et al. (4) demonstrated heavy infected red blood cell (iRBC) sequestration in the cerebrovasculature of children who died of CM, which was often accompanied by intra- and perivascular pathology, including ring hemorrhages. Further studies

▶ Related Commentary: https://doi.org/10.1172/JCI135510

Authorship note: BAR and MM are co–first authors. DBM and SKP are co–senior authors.
Conflict of interest: The authors have declared that no conflict of interest exists.

Submitted: September 17, **Published:** February 17, 2020.
Reference information: *J Clin Invest*. https://doi.org/10.1172/JCI133474.

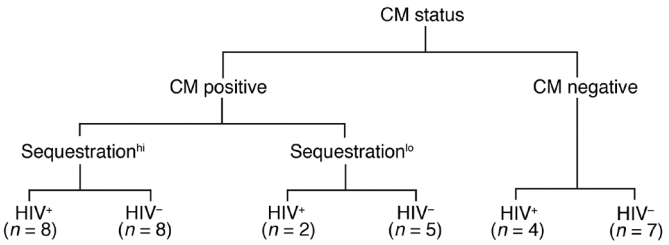

Figure 1. Flow chart of patient classification. Patients were first grouped by antimortem CM status as diagnosed on admission to the Paediatric Research Ward. Patients were further subcategorized based on analysis of postmortem H&E-stained sections from the same cerebral biopsy sample analyzed by MP-IHC. An iRBC sequestration cut-off of 23.1% between "hi" and "lo" was prospectively determined based on previous studies. These 3 groups were then further subcategorized based on HIV status.

identified polymorphisms in immune modulating genes leading to protection or predisposition to CM, production of inflammatory cytokines (e.g., IFN-γ and TNF), neuro- and systemic inflammation, cerebral edema and increases in intracranial pressure, blood-brain barrier (BBB) dysfunction, and fatal brainstem herniation (5–12). These observations led to the generally accepted hypothesis that iRBC sequestration in the cerebrovasculature and the resulting sequelae, including mechanical obstruction, inflammation, impaired vasoregulation, and BBB dysregulation, causes this clinical syndrome (4). Clinical trials of various therapies attempting to target the downstream effects of this mechanism have been carried out (13), including trials of dexamethasone to decrease cerebral edema (14, 15), intravenous immunoglobulin to reverse iRBC sequestration (16), TNF-specific monoclonal antibodies to decrease immune activation (17), pentoxifylline to decrease TNF production and improve RBC deformability (18, 19), nitric oxide (NO) inhalation to modulate endothelial activation (20, 21), heparin or aspirin to counter a prothrombotic state (22), osmotic agents to decrease cerebral edema and reduce intracranial pressure (ICP) (23–25), and therapies to expand intravascular volume to ameliorate acidosis (26, 27). Unfortunately, none of these trials improved clinical outcomes (13, 20, 28).

An existing mouse model for CM, experimental CM (ECM), shares many features with the human disease. Indeed, several studies using a variety of imaging modalities, including MRI, provided evidence of vasogenic brain swelling, BBB dysfunction, and fatal brainstem herniation in ECM (29–32), similar to observations in children with CM by MRI (12, 33). However, the mouse model suggests an alternative mechanism of pathology. ECM requires cross-presentation of parasite antigens on MHC-I by the endothelial brain vasculature and targeting of this vasculature by $CD3^+CD8^+$ T cells (34, 35). To date, only 2 studies have addressed the recruitment of $CD8^+$ T cells in the cerebrovasculature of children with CM. One study described monocyte, platelet, and neutrophil brain infiltrates but did not find $CD8^+$ T cells; possibly due to the sensitivity of the methodology employed and the relative poor quality of the CD8-specific antibodies available at the time (36). A second, more recent study reported small numbers of $CD8^+$ cells were present equally in the brains of children who died of CM and those who died of other causes (37). However, this study failed to rigorously distinguish $CD3^+CD8^+$ T cells from infiltrating $CD3^-CD8^+$ monocytes and was underpowered to find statistical significance. Thus, a critical gap in our knowledge of CM in children is whether a pattern of $CD3^+CD8^+$ T cell accumulation, resembling that observed in the murine model of CM, exists in the brains of children who died of CM.

Herein, we describe the results of a multiplex immunohistochemistry (MP-IHC) analysis of brain tissue samples from children who died from CM or other causes and were either HIV^+ or HIV^-. We provide definitive evidence that effector $CD3^+CD8^+$ T cells are present in the brains of children who died of CM. In addition, we show that the number of $CD3^+CD8^+$ T cells is even greater in the brains of HIV-infected children with CM, suggesting that HIV coinfection can influence CM. $CD3^+CD8^+$ T cells loaded with granzyme B were distributed both in the lumen of the venous vasculature in close association with the endothelium as well as on the abluminal side of vessels in the perivascular spaces. This distribution recapitulates the distribution of $CD3^+CD8^+$ T cells in the brain vasculature of mice with ECM, a disease in which $CD3^+CD8^+$ T cells play an essential role in mediating brain pathology. These observations open new avenues for adjunctive treatment for CM that involve modulating $CD3^+CD8^+$ T cells with a wealth of available T cell targeting therapeutics.

Results

Patients. Twenty-three CM^+ children (Patients 1–23) who met the WHO's criteria for CM diagnosis, namely coma and peripheral parasitemia, with no other obvious cause of coma, and 11 CM^- children (Patients 24–34) who did not meet these criteria were analyzed (Table 1). Coma was determined by the Blantyre Coma Scale (BCS) (described in Supplemental Table 1; ref. 2; supplemental material available online with this article; https://doi.org/10.1172/JCI133474DS1), with a score equal to or less than 2 (an unrousable coma) required for diagnosis of CM. The HIV infection status of the 34 children and viral titers (when available) are provide in Table 1. Peripheral parasitemia assessed by thick blood smear and *P. falciparum* histidine-rich protein-2 (HRP2) levels in serum (38), a measure of total body parasite loads, are given in Table 1. Because sequestration of iRBCs is a hallmark of CM, the percentage of blood vessels in each section with sequestered iRBCs was also quantified. Representative images depict high sequestration levels (Seq^{hi}) in the brains of CM^+ HIV^- (Supplemental Figure 1A) and CM^+ HIV^+ children (Supplemental Figure 1B). Examples of low to no sequestration (Seq^{lo} or Seq^0) are given for CM^+ HIV^-, CM^- HIV^-, and CM^- HIV^+ children, respectively (Supplemental Figure 1, C–E). Collectively, CM status, iRBC sequestration levels, and HIV status were used to define 6 groups of children (Figure 1 and Table 1): CM^+ Seq^{hi} HIV^- (Patients 1–8), CM^+ Seq^{hi} HIV^+ (Patients 9–16), CM^+ Seq^{lo} HIV^- (Patients 17–21), CM^+ Seq^{lo} HIV^+ (Patients 22 and 23), CM^- Seq^0 HIV^- (Patients 24–30), and CM^- Seq^0 HIV^+ (Patients 31–34). The majority of the samples analyzed were collected by the Blantyre Malaria Project (BMP) (see Methods); however, the CM^- Seq^0 HIV^- group also included samples acquired from the Human Brain Collection Core (HBCC) (see Methods and Supplemental Table 2).

Multiplex immunohistochemical analysis. We performed quantitative MP-IHC to immunologically profile the cerebrovasculature

Table 1. Clinical and laboratory findings for autopsy cases from the Blantyre Malaria Project and the Human Brain Collection Core

	Clinical CM[A]	BCS[B]	Age, months	Sex	Vessel sequestration[C]	Peripheral parasitemia[D]	HRP2[E]	HIV[F]	HIV VL[G]
1	Yes	2	25	F	>95%	9.7	16.7	Neg	–
2	Yes	2	44	F	>95%	0.5	15.3	Neg	–
3	Yes	1	39	F	>95%	81.8	NA	Neg	–
4	Yes	0	84	F	80%	782.3	3.7	Neg	–
5	Yes	1	25	F	80%	104.2	14.6	Neg	–
6	Yes	1	51	F	70%	126.0	15.4	Neg	–
7	Yes	0	15	M	70%	736.1	2.9	Neg	–
8	Yes	1	42	F	30%	0.4	6.4	Neg	–
9	Yes	1	156	M	>95%	35.4	22.5	Pos	8.4
10	Yes	1	103	F	>95%	315.0	15.6	Pos	26.4
11	Yes	1	144	M	>95%	308.7	13.6	Pos	1.6
12	Yes	1	79	M	>95%	48.0	3.6	Pos	7.8
13	Yes	1	106	F	>95%	201.8	3.5	Pos	4.4
14	Yes	1	72	F	>95%	1.7	23.5	Pos	15.1
15	Yes	1	11	F	80%	699.3	2.7	Pos	88.1
16	Yes	1	96	F	70%	78.9	23.5	Pos	40.6
17	Yes	1	25	M	5%	0.5	14.0	Neg	–
18	Yes	0	60	F	<5%	0.3	0.0	Neg	–
19	Yes	2	39	M	<5%	91.0	0.6	Neg	–
20	Yes	0	27	M	0%	652.9	12.4	Neg	–
21	Yes	0	17	M	0%	97.7	0.1	Neg	–
22	Yes	1	41	M	5%	324.8	1.5	Pos	NA
23	Yes	1	35	M	0%	159.4	0.4	Pos	11.7
24	No	1	33	F	0%	0.1	–	Neg	–
25	No	5	42	M	0%	0	–	Neg	–
26	No	[H]	4.8	M	0%	0	–	Neg	–
27	No	[H]	6	F	0%	0	–	Neg	–
28	No	[H]	50.4	M	0%	0	–	Neg	–
29	No	[H]	24	F	0%	0	–	Neg	–
30	No	[H]	99.6	M	0%	0	–	Neg	–
31	No	5	144	F	0%	NA	–	Pos	NA
32	No	0	36	F	0%	0	–	Pos	73.6
33	No	3	41	F	0%	0	–	Pos	NA
34	No	0	121	M	0%	0	–	Pos	NA

Grey indicates HIV negative; white indicates HIV positive. [A]Antimortem diagnosis based on the WHO guidelines for clinical diagnosis (see Methods). In some cases, there were suspected or identified nonmalarial causes of death on autopsy. [B]Blantyre Coma Score (see Methods and Supplemental Table 1). [C]Vessel sequestration within the serial section proximal to the one analyzed by IHC. [D]10^3 parasites/μL. [E]10^6 ng/mL. [F]HIV status from rapid diagnostic test (see Methods). [G]Viral load (10^4 copies/mL) based on retrospective analysis of available plasma. NA, Data not collected or unavailable. [H]HBCC tissue from NIMH, not evaluated on BCS. Further data, including cause of death, in Supplemental Table 2.

of all 34 samples. The panel of antibodies used included ones specific for CD3 (a pan–T cell marker), CD8 (cytotoxic T cells), IBA1 (a microglia/macrophage marker), CD68 (myeloid cell activation marker), CD31 (endothelial cell marker), and SMA (smooth muscle actin, a marker of arterial vasculature) (Supplemental Table 3). The DNA-binding dye DAPI was included to identify cell nuclei. Representative images of venous vasculature in brain sections from HIV$^-$ children either CM$^+$ Seq^{hi} (Figure 2A), CM$^+$ Seq^{lo} (Figure 2B), or CM$^-$ Seq^0 (Figure 2C) stained with DAPI and antibodies specific for CD31, CD8, and CD3 are shown. CD3$^+$CD8$^+$ T cells were observed juxtavascular to CD31$^+$ venous vascular endothelial cells in both CM$^+$ Seq^{hi} and CM$^+$ Seq^{lo} but not in CM$^-$ Seq^0 patients (Figure 2, A–C). Juxtavascular CD3$^+$CD8$^+$ T cells were further categorized as luminal if they were intravascular, or abluminal if they were within the perivascular space. The area of each vessel was determined and used to calculate the number of luminal, abluminal, and total CD3$^+$CD8$^+$ T cells per μm^2 of the venous aspect of the vasculature (Figure 2, D–F). The number of CD3$^+$CD8$^+$ T cells was significantly increased along the luminal surface of cerebrovasculature in CM$^+$ Seq^{hi} children relative to CM$^+$ Seq^{lo} (P = 0.011, 95% CI 0.041–1.54) and CM$^-$ Seq^0 children (P = 0.004, 95% CI 0.471–1.50). Furthermore, the difference between the total number of CD3$^+$CD8$^+$ T cells between CM$^+$ Seq^{hi} HIV$^-$ and CM$^-$ Seq^0 HIV$^-$ approached significance (P = 0.057, 95% CI 0.135–2.17) (Figure 2F).

Currently, it is hypothesized that the intracranial hypertension observed in CM results from impaired venous blood flow

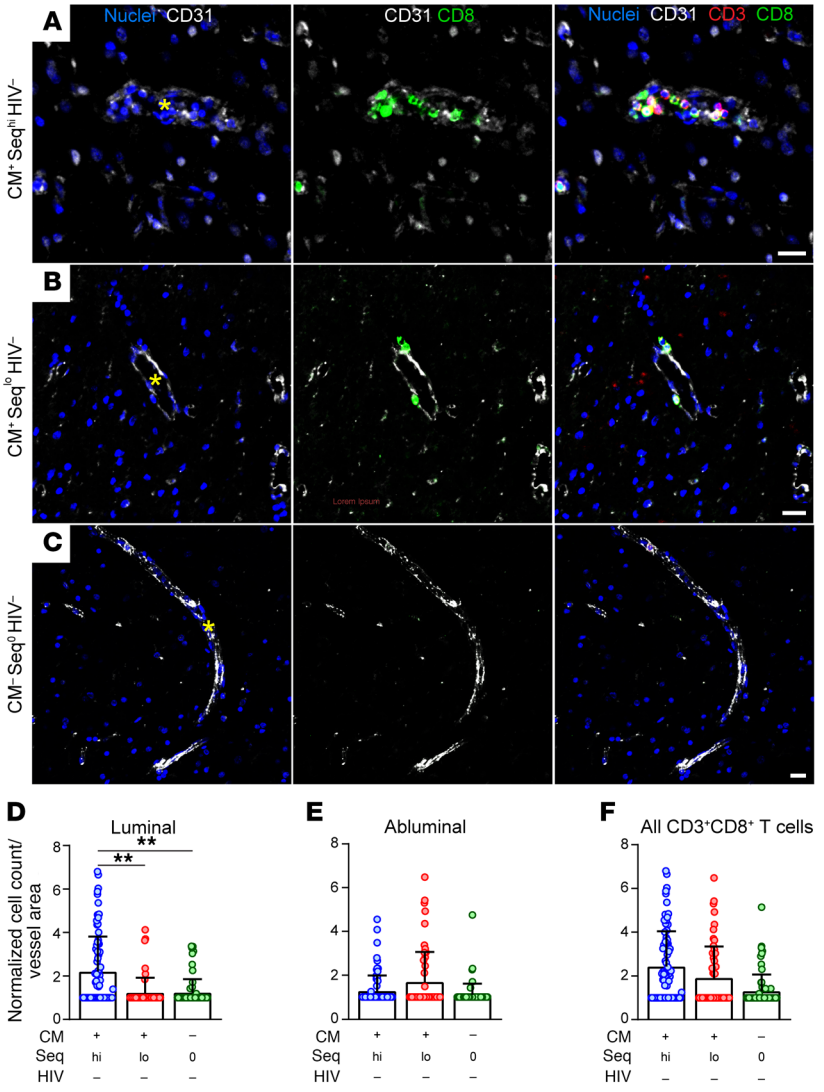

Figure 2. CD3⁺CD8⁺ T cells within venous cerebrovasculature of CM children. Shown are representative images of brain sections from CM⁺ Seq^{hi} HIV⁻ (**A**), CM⁺ Seq^{lo} HIV⁻ (**B**), and CM⁻ Seq^{0} HIV⁻ (**C**) patients. Images depict the distribution of CD3⁺ (red) CD8⁺ (green) T cells in relation to CD31⁺ (white) cerebrovasculature. DAPI-stained cell nuclei are shown in blue. Scale bars: 20 μm. Yellow asterisks denote the vascular lumen. Normalized counts of luminal, abluminal, and total CD3⁺CD8⁺ T cells per vessel area ($\log_2$((number of cells/μm^2/10^4) + 2)) are described in **D**–**F**. Each symbol within a plot represents the normalized count of CD3⁺CD8⁺ T cells per vessel area for 1 of the 20 vessels examined for each child. Luminally, a significant increase in CD3⁺CD8⁺ T cells/vessel area was observed in CM⁺ Seq^{hi} (n = 8) patient brain sections relative to CM⁺ Seq^{lo} (n = 5; FDR P = 0.010) and CM⁻ Seq^{0} (n = 7; FDR P = 0.004) sections (**D**). P values were obtained via post hoc analysis using the difflsmeans function under FDR correction conditions following mixed-effects modeling with the lmer function. Significant differences remained so under bootstrap conditions 100% of the time when any normalized cell count for a single vessel was removed or when all vessels for any 1 child were removed. Error bars represent mean ± SD. Asterisks denote statistical significance: FDR **$P \leq 0.01$.

due to iRBC and immune cell sequestration within venous vasculature in which flow velocities are already significantly decreased compared with arterial vasculature (39). We therefore examined whether there were differences in CD3⁺CD8⁺ T cell accumulation in arteries versus veins. We found that CD3⁺CD8⁺ T cells were present in larger numbers in veins as compared with arteries in CM⁺ Seq^{hi} HIV⁻ children, irrespective of HIV status (Figure 3A, $P < 0.001$, 95% CI –1.02 to –0.37, and Figure 3B $P = 0.035$, 95% CI –0.73 to –0.08) but accumulated equally in arteries and veins in CM⁺ Seq^{lo} HIV⁻ children (Figure 3C). Few CD3⁺ CD8⁺ T cells were observed in CM⁻ Seq^{0} HIV⁻ patient samples (Figure 3D), and most of these were in a single US control patient who died of acute myocarditis. There was no evidence of CD3⁺CD8⁺ T cells in the brain parenchyma. HIV infection alone did not bias CD3+CD8+ distribution (Figure 3E).

To confirm that the juxtavascular CD3⁺CD8⁺ T cells were effector cells, we used confocal microscopy to image expression of granzyme B, CD31, and CD8 using specific antibodies (Supplemental Table 3) in sections serial to those used in the MP-IHC experiment (Figure 4, A–D). CD8⁺ T cells expressing the effector molecule granzyme B were found engaged with or adjacent to the wall of CD31⁺ cerebrovasculature, some of which contained RBCs. CD8⁺ T cells were also observed releasing granzyme B extracellularly (Figure 4D), which suggests target cell engagement. Collectively, these data provide strong evidence that granzyme B⁺ effector CD3⁺CD8⁺ T cells target cerebrovasculature in the brains of children who died from CM.

We next assessed the influence of HIV infection on the accumulation of CD3⁺CD8⁺ T cells in the brain samples (Figure 5A–C). For CM⁺ Seq^{hi} children, HIV coinfection was associated with a significant increase in the total number of cerebrovascular CD3⁺CD8⁺ T cells and these localized more abluminally than luminally (Figure 5D–F). HIV infection independent of CM also showed abluminal accumulation of CD3⁺CD8⁺ T cells (Figure 5E).

There was no detectable staining for HIV p24 in any of the samples. In addition, hallmark features of cerebral HIV infection, such as multinucleated giant cells and microglial nodules, were not observed on H&E-stained brain sections (Supplemental Figure 1). Thus, the distribution of CD3⁺CD8⁺ T cells in HIV⁺ children, both CM⁺ and CM⁻, was not explained by the presence of detectable viral antigen.

We imaged and quantified the luminal, abluminal, and total cell number of activated monocytes/macrophages (IBA1⁺CD68⁺) around the same cerebral blood vessels profiled in Figure 2 for CD3⁺CD8⁺ T cells (Figure 6). A greater total number of activated IBA1⁺CD68⁺ monocytes/macrophages localized to the cerebrovasculature of CM⁺ Seq^{hi} HIV⁻ children when compared with CM⁺ Seq^{lo} HIV⁻ and CM⁻ Seq^{0} HIV⁻ children, and these cells were found primarily along the luminal surface (Figure 6, A–D). Interestingly, HIV coinfection shifted the distribution of activated IBA1⁺CD68⁺ monocytes/macrophages away from the luminal surface in CM⁺ Seq^{hi} patients (Figure 6, E–H) — a pattern also observed with CD3⁺CD8⁺ T cells (Figure 5). Collectively, these data demonstrate that high iRBC sequestration is associated with a strong innate cerebrovascular immune response

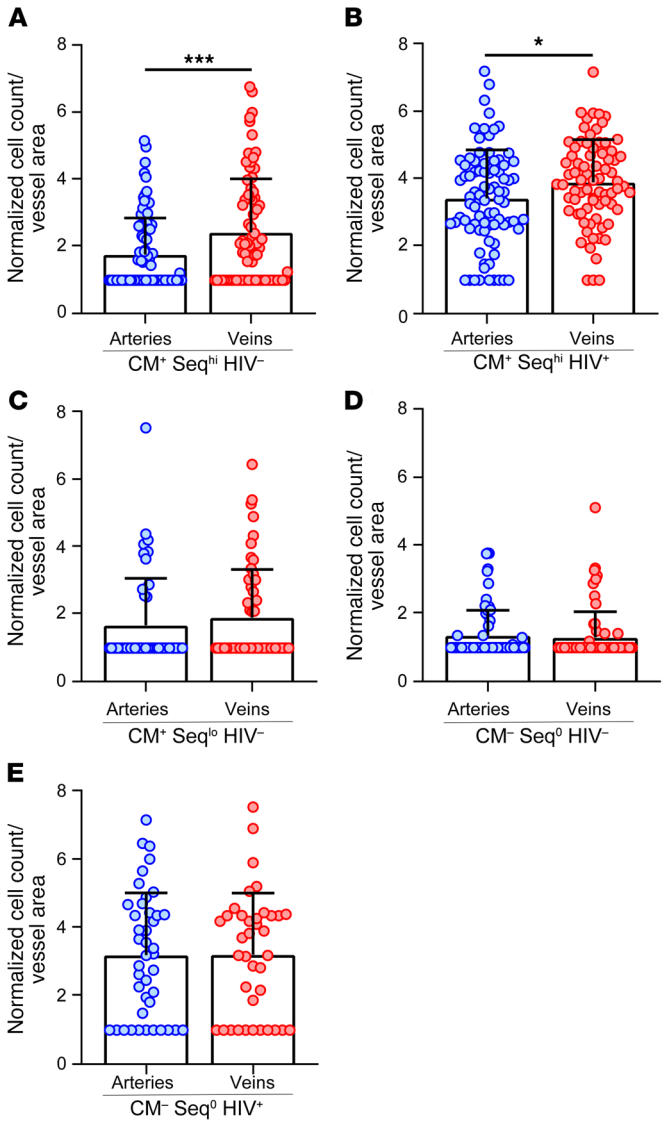

Figure 3. Quantification of CD8⁺ T cells in cerebral arteries versus veins. Normalized counts of CD3⁺CD8⁺ T cells per vessel area ($\log_2$((number of cells/ $\mu m^2/10^4$) + 2)) are described in **A**–**E**. Each symbol within a plot represents the normalized count of CD3⁺CD8⁺ T cells per vessel area for 1 of the 20 vessels examined for each child with the color denoting the vessel type (artery: blue; vein: red). A significant increase in venous CD3⁺CD8⁺ T cell counts was observed for CM⁺ Seq^{hi} HIV⁻ (**A**, $n = 8$; FDR $P < 0.001$) and CM⁺ Seq^{hi} HIV⁺ (**B**, $n = 8$; FDR $P = 0.035$). No significant difference in normalized CD3⁺CD8⁺ T cell counts was observed between arteries and veins for CM⁺ Seq^{lo} HIV⁻ (**C**, $n = 5$), CM⁻ Seq^0 HIV⁻ (**D**, $n = 7$), or CM⁻ Seq^0 HIV⁺ (**E**, $n = 4$). *P* values were obtained via post hoc analysis using the diffslsmeans function under FDR correction conditions following mixed-effects modeling with the lmer function. Significant differences remained so under bootstrap condition 100% of time when any normalized cell count for a single vessel was removed or when all vessels for any 1 child were removed. Error bars represent mean ± SD. Asterisks denote statistical significance: FDR $^*P \le 0.05$; $^{***}P \le 0.001$.

and that HIV coinfection influences the localization (luminal versus abluminal) of this response.

Discussion

Using recently developed, sensitive MP-IHC methods, we identified juxtavascular effector CD3⁺CD8⁺ T cells in brain sections from 69% (9/13) of children who died of CM but were HIV⁻. These CD8⁺ T cells appeared to be engaged with the vessel wall and were loaded with the lytic effector molecule, granzyme B, that was sometimes deposited extracellularly, suggesting target cell recognition. It is notable that CD3⁺CD8⁺ T cells were identified in a large percentage of children even though the sections analyzed represented only a very small snapshot of the brain. Indeed, because we only examined a biopsy from 1 brain region per patient, it is possible that we missed the pathology in the other 4 patients due to heterogenous CD3⁺CD8⁺ T cell infiltration. We observed an unexpected impact of sequestration on the number and localization of CD3⁺CD8⁺ T cells, suggesting that variables that influence sequestration, including activation of the endothelium, may also affect T cell engagement with the endothelium. Additionally, activated IBA1⁺CD68⁺ myeloid cells were recruited to the luminal surface of cerebrovasculature in CM patients, matching the distribution of CD3⁺CD8⁺ T cells. These may contribute to the removal of adherent iRBCs from the vascular lumen, a function they provide in mice with ECM (29). Importantly, T cell and innate immune cell accumulation occurred independently of HIV infection, although coinfection significantly enhanced juxtavascular CD3⁺CD8⁺ T cells in the brain and influenced their distribution. Furthermore, we demonstrated increased accumulation of CD3⁺CD8⁺ T cells in venous versus arterial vasculature of CM⁺ Seq^{hi} HIV⁻ and CM⁺ Seq^{hi} HIV⁺ patients. We postulate that the slower blood flow in veins promotes increased accumulation of parasite-specific T cells along this type of blood vessel. In fact, iRBCs were also shown to sequester preferentially along venous vasculature (40), which likely facilitates endothelial antigen acquisition and cross-presentation to CD8⁺ T cells.

Our study also showed that untreated HIV coinfection with CM was associated with larger numbers of CD3⁺CD8⁺ T cells abluminally distributed around brain vasculature, suggesting extravasation. This phenomenon did not appear to be linked to the presence of HIV antigen as we were unable to detect HIV p24 in brain sections. However, we cannot rule out the possibility that the amount of HIV antigen was below our level of detection, that HIV-specific T cells had controlled the virus, or that the virus had localized to other brain regions not sampled in our study. The CM⁺ HIV⁺ children in the BMP cohort were older than the CM⁺ HIV⁻ children (99 versus 32 months) (38), as were the children in our study. Because a majority of children with untreated HIV die early in life, those that survive to the age of 7 to 8 years are presumably better able to control HIV progression. In all cases, an HIV-positive diagnosis was identified concurrent with admission to the Paediatric Research Ward (PRW) for suspected CM or on retrospective analysis; therefore, none of the children were on HIV therapies at the time of death. Factors that influence a child's response to HIV might also affect CD8⁺ T cell responses during CM.

Our observations point to a role for CD8⁺ T cells in human CM pathology. In mice, CD8⁺ T cells were shown to be required for ECM where parasite-specific CD8⁺ T cells arrest on the luminal and abluminal surfaces of venous cerebrovasculature following recognition of parasite antigen cross-presented by endothelial MHC-I (29, 34, 35, 41). ECM is also dependent on granzyme B, a lytic effector molecule that we observed in CD8⁺ T cells targeting the vessel wall of CM patients (42). It is remarkable that the jux-

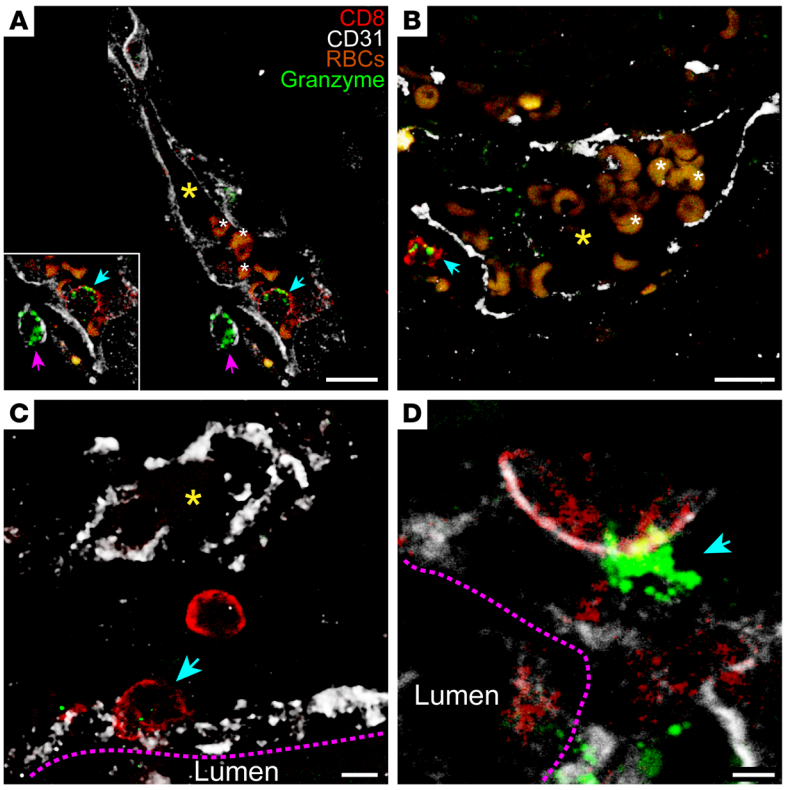

Figure 4. Granzyme B–loaded CD8⁺ T cells target cerebrovasculature during CM. Shown are representative confocal images captured from a CM⁺ Seq^{hi} HIV⁻ patient brain section. Images depict the distribution of granzyme B (green) and CD8⁺ T cells (red) in relation to CD31⁺ (white) cerebrovasculature and autofluorescent RBCs (orange). Representative RBCs in **A** and **B** are denoted with small white asterisks. The vascular lumen is denoted with large yellow asterisks or the word "lumen." The dotted pink lines in **C** and **D** delineate the border of the blood vessel walls. Cyan arrowheads denote granzyme B⁺ CD8⁺ T cells engaged with (**A**–**C**) or depositing granzyme B⁺ onto (**D**) CD31⁺ vasculature. The pink arrowheads in **A** denote a CD8⁻ granzyme B⁺ cell. Scale bars: 10 μm (**A** and **B**), 4 μm (**C**), and 2 μm (**D**).

tavascular distribution of CD8⁺ T cells in children perfectly mirrored the distribution observed in the mouse model of CM. Given these observations, it is encouraging that drugs that target T cells have proven effective in preventing and even reversing ECM in mice (29, 32, 43). We demonstrated that the glutamine antagonist, 6-diazo-5-oxo-L-norleucine (DON), which targets the metabolism of activated T cells, is highly efficacious in treating mice late in the disease, when it has progressed to a point where significant brain swelling and BBB dysfunction have occurred (32, 43). Another adjunctive therapy for CM was suggested by our finding that blocking vascular adhesion of CD8⁺ T cells in the brains of mice using VLA-4– and LFA-1–specific antibodies rescued mice from late-stage ECM (29, 44). Indeed, such antibodies have been approved by the FDA for use in humans. Collectively, our findings raise the exciting possibility that drugs developed over recent years to target T cell functions in both cancer and autoimmunity may be candidates for adjunctive therapies in CM.

Herein we provided definitive evidence for the presence of CD8⁺ T cells in appreciable and significant numbers in contact with the cerebral vasculature of children who died from cerebral malaria. Our findings point to a mechanism by which CD8⁺ T cells function in the development of CM based on the extraordinary similarities in the distribution of CD8⁺ T cells in the brains of children with CM to that of mice with ECM. These observations may ultimately give way to a paradigm shift in the development of adjunctive therapies, finally providing rescue from this deadly disease.

Methods

Clinical data

Clinicopathological study and consent. Brain samples from 31 children were obtained from a parent study of the clinicopathological correlates and pathogenesis of fatal cerebral malaria carried out between 1996 and 2010 in the PRW of Queen Elizabeth Central Hospital in Blantyre, Malawi, and run by the Blantyre Malaria Project (BMP) and the Malawi-Liverpool-Wellcome Trust Clinical Research Programme (MLW) as previously described (4, 38, 45, 46). The study was approved by the institutional review boards (IRBs) of the University of Malawi College of Medicine, Michigan State University, and the Brigham and Women's Hospital (47). Full autopsies were carried out on 103 children between the age of 6 months and 12 years who died of CM or other causes. In the parent case-control study, children were evaluated and included in the CM arm upon meeting the criteria of CM defined by the WHO (2). In the present analysis, we received 3 to 4 serial sections (1–2 cm² × 5-μm thick) cut from paraffin-embedded, formalin-fixed tissue mostly obtained from either the occipital or parietal regions of the brain. These samples and the associated clinical and laboratory test results (including BSC, age, sexual phenotype, peripheral parasitemia and *Pf*HRP2 levels, and HIV status and viral load, described below) are reported in Table 1. An additional 5 samples from African-American children aged 0.4 to 8.3 years old were obtained from the Human Brain Collection Core (HBCC) at the National Institute of Mental Health (NIMH), collected between 1994 and 2008, and prepared in the same manner as above (Supplemental Table 2). Of the 31 BMP samples, 2 were excluded, the first due to poor tissue quality (CM⁺ HIV⁻) and the second due to inability to confirm HIV status (CM⁺).

Blantyre coma scale. The BCS was designed to assess malarial coma in children through motor and verbal responses as well as eye movements. Scores range from 0 to 5, with 0 indicating the most severe conditions and any score less than 5 considered abnormal. A score of 2 or less (an unrousable coma) is required for diagnosis of CM (Supplemental Table 1 and ref. 2).

PfHRP2 measurement. Hochman et al. measured *Pf*HRP2 levels using enzyme-linked immunosorbent assay of archived frozen plasma (39). The results of these measurements were supplied to us along with the other clinical data.

HIV status and viral loads. Widespread antiretroviral therapy (ART) and quantification of CD4⁺ T cells in peripheral blood were uncommon in Malawi over the duration of the parent study. Voluntary HIV counseling and testing were incorporated in 2001. HIV testing was performed using 2 rapid tests, Uni-Gold Recombigen

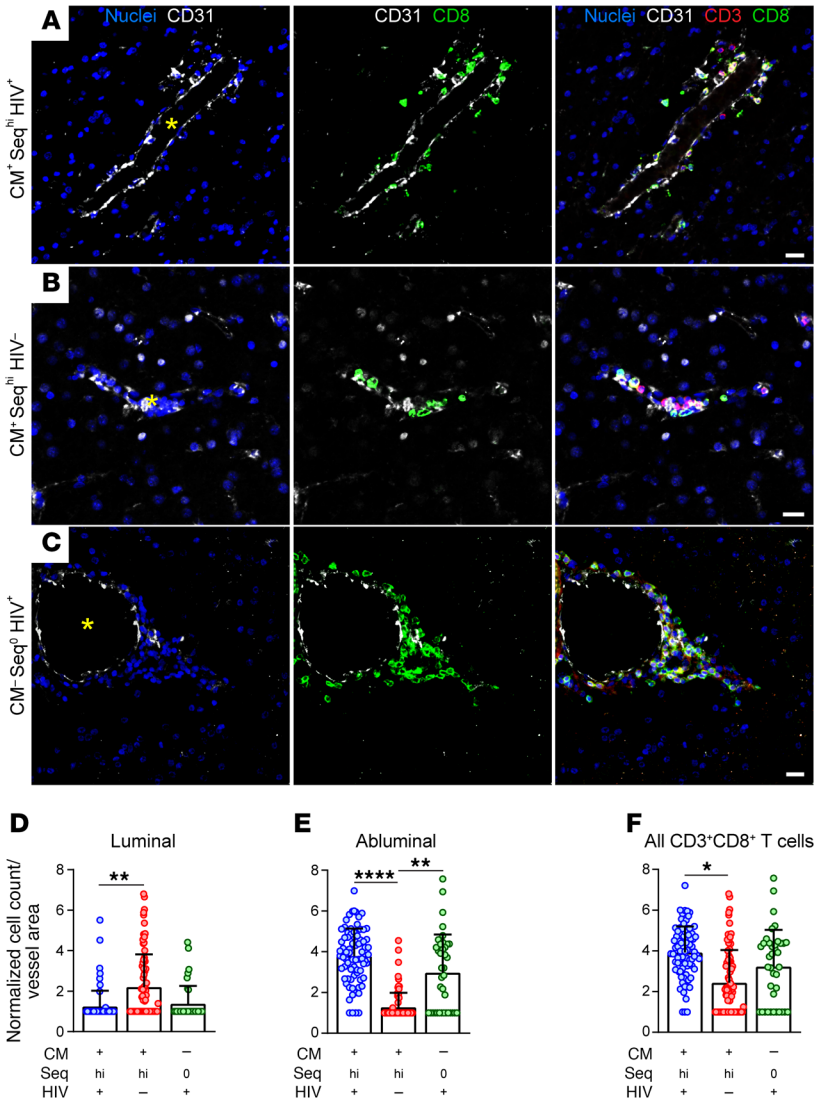

Figure 5. Impact of HIV infection on the accumulation of CD8⁺ T cells in venous cerebrovasculature. Representative images of brain sections from CM⁺ Seq^{hi} HIV⁺ (**A**), CM⁺ Seq^{hi} HIV⁻ (**B**), and CM⁻ Seq^{0} HIV⁺ (**C**) children. Images show the distribution of CD3⁺ (red), CD8⁺ (green) T cells in relation to CD31⁺ (white) cerebrovasculature. DAPI-stained cell nuclei are shown in blue. Yellow asterisks denote the vascular lumen. Scale bars: 20 μm. Normalized counts of luminal, abluminal, and total CD3⁺CD8⁺ T cells/vessel area (log_2((number of cells/μm²/10⁴) + 2) are provided in **D**–**F**. Each symbol represents the number of CD3⁺CD8⁺ T cells/vessel area for 1 of the 20 vessels examined per child. In CM⁺ Seq^{hi} children, HIV coinfection was associated with a decrease in CD3⁺ CD8⁺ T cells/vessel area, luminally (**D**, n = 8 for both; FDR P = 0.004). Conversely, in CM⁺ Seq^{hi} children, HIV coinfection was associated with an increase in CD3⁺CD8⁺ T cells/vessel area abluminally. HIV⁺ cases with (n = 8) or without CM (n = 4) also showed significantly more CD3⁺CD8⁺ T cells/vessel area abluminally than cases without HIV (n = 8) coinfection (**E**, FDR $P < 0.0001$ and FDR $P < 0.005$, respectively). Furthermore, CM⁺ Seq^{hi} HIV⁺ children had a greater total number of CD3⁺ CD8⁺ T cells/vessel area compared with CM⁺ Seq^{hi} HIV⁻ (**F**, FDR $P <$ 0.017). P values were obtained via post hoc analysis using the diffIsmeans function under FDR correction conditions following mixed-effects modeling with the lmer function. Significant differences remained so under bootstrap conditions 100% of time when any normalized cell count for a single vessel was removed or when all vessels for any 1 child were removed. Error bars represent mean ± SD. Asterisks denote statistical significance: FDR *$P \le 0.05$; **$P \le 0.01$; ****$P < 0.0001$.

HIV-1/2 (Trinity Biotech) and Determine HIV-1/2 (Inverness Medical) (12). Plasma from autopsy cases not tested prior to death and archived specimens from 1996 to 2000 were retrospectively analyzed, with IRB approval, by Hochman et al. (38). The results of this analysis were subsequently provided to us with the rest of the clinical data. All patients with clinically defined CM prior to autopsy had HIV antibody testing. Of the 103 children autopsied, some children with another cause or an indeterminate cause of death prior to autopsy were not tested for HIV or testing could not be confirmed. Of the remaining 96 autopsy cases, 20 with definitive testing were HIV⁺. All 14 HIV⁺ cases with archived plasma had quantifiable HIV loads (Abbott m2000 system). The tissues analyzed in this study represent a subset of the autopsy series, including 10 of the 14 HIV⁺ children with archived plasma.

Tissue analysis

Pathology. One brain section of the series for each patient was H&E stained and evaluated for gross pathological changes and percentage of parasite sequestration (Supplemental Figure 1). The pathologist was blinded to all clinical data. Slides were scanned using a NanoZoomer-XR Digital slide scanner (Hamamatsu). Analysis was performed in NDP.view (Hamamatsu). Based on the percentage of vessels within the slice exhibiting sequestration (Seq), sections were classified as Seq^{hi}, Seq^{lo}, or Seq^{0}. Seq^{hi} brain sections had iRBCs in at least 23.1% of the cerebral vasculature, whereas Seq^{0} sections had no detectible iRBCs in the vessels and no peripheral parasitemia. The cutoff between "hi" and "lo" was prospectively determined based on previous findings in autopsy studies of CM (40).

Immunohistochemistry tissue preparation. MP-IHC was performed on 5-μm-thick paraffin sections sourced from postmortem cerebral samples. The sections were first deparaffinized using standard xylene/ethanol rehydration protocol followed by antigen unmasking using standard heat-mediated antigen retrieval in 10 mM Tris/EDTA buffer pH 9.0. The sections were then incubated with Human BD Fc Blocking solution (BD Biosciences) to saturate endogenous Fc receptors, and then in True Black Reagent (Biotium) to quench intrinsic tissue autofluorescence. The sections were then immunoreacted for 1 hour at room temperature using 1–5 μg/mL cocktail mixture of the following immunocompatible primary antibodies: mouse IgG1 anti-CD3 in combination with mouse IgG2b anti-CD8 (both from

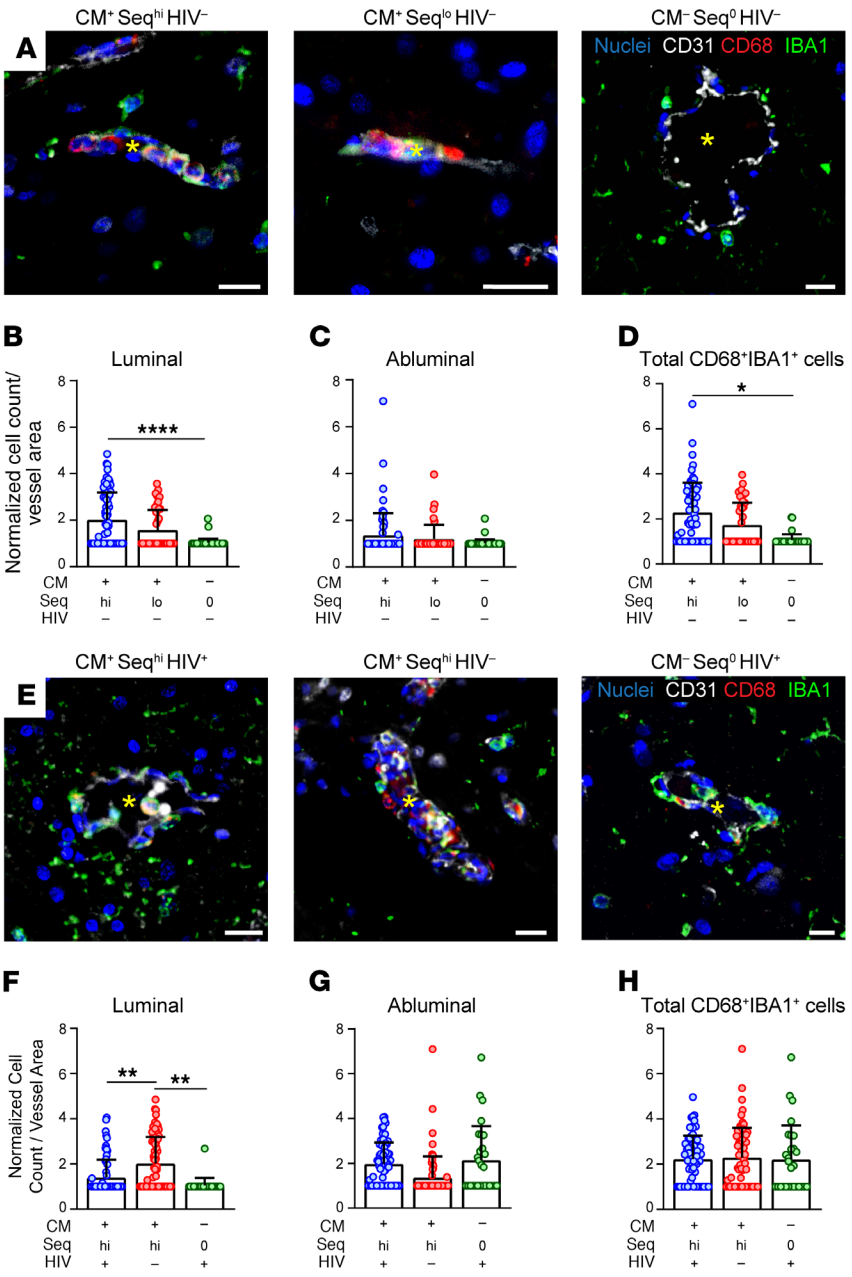

Figure 6. Activated CD68$^+$IBA1$^+$ monocytes/macrophages in the venous cerebrovasculature. Representative images of brain sections from CM$^+$ Seq^{hi} HIV$^-$, CM$^+$ Seq^{lo} HIV$^-$, and CM$^-$ Seq^0 HIV$^-$ (**A**) patients and CM$^+$ Seq^{hi} HIV$^+$, CM$^+$ Seq^{hi} HIV$^-$, and CM$^-$ Seq^0 HIV$^+$ (**E**) patients. Images show the distribution of IBA1$^+$ (green), CD68$^+$ (red) monocytes/macrophages in relation to CD31$^+$ (white) cerebrovasculature and DAPI-stained cell nuclei (blue). Yellow asterisks denote the vascular lumen. Scale bars: 20 μm. Normalized counts of luminal, abluminal, and total CD68$^+$IBA1$^+$ inflammatory monocytes/macrophages/vessel area ($\log_2$((number of cells/μm^2/10^4) + 2) in the same ROIs used previously are given in **B**–**D** and **F**–**H**. Each symbol represents the number of CD68$^+$IBA1$^+$ cells/vessel area for each of the 20 vessels examined per child. There were significantly more activated monocytes/macrophages luminally in CM$^+$ (n = 8) versus CM$^-$ (n = 7) children (**B**, FDR $P < 0.0001$). CM$^+$ Seq^{lo} HIV$^-$ in **B**–**D**, n = 5. This is also reflected when comparing total cell numbers between both groups (**D**, FDR $P < 0.030$). Comparison of CM patients with (n = 8) and without (n = 8) HIV shows that CM alone promotes recruitment of activated monocytes/macrophages on the luminal aspect of cerebrovasculature (**F**, FDR $P < 0.006$). This observation is also evident when comparing CM$^+$ Seq^{hi} HIV$^-$ and CM$^-$ Seq^0 HIV$^+$ (n = 4) patients (**F**, FDR $P < 0.002$). P values were obtained via post hoc analysis using the difflsmeans function under FDR correction conditions following mixed-effects modeling with the lmer function. Significant differences remained so under bootstrap conditions 100% of the time when any single vessel normalized cell count was removed or when all vessels for any 1 child were removed. Error bars: mean ± SD. Asterisks denote statistical significance: FDR *$P \le 0.05$; **$P \le 0.01$; ****$P < 0.0001$.

Thermo Fisher Scientific/Invitrogen) to identify infiltrating CD3$^+$CD8$^+$ T cells, mouse IgG3 anti-CD68 (Abcam) in combination with chicken IgY anti-Iba1 (Synaptic Systems) to identify infiltrating macrophages, and guinea pig IgG anti-CD31 (Synaptic Systems) in combination with mouse IgG2a anti-SMA (GeneTex) to identify endothelial cells and pericytes, respectively (Supplemental Table 3). This step was followed by washing off excess primary antibodies in PBS supplemented with 1 mg/mL BSA and staining the sections using a 1 μg/mL cocktail mixture of the appropriately cross-adsorbed secondary antibodies (purchased from either Thermo Fisher Scientific/Invitrogen or Li-Cor Biosciences) conjugated to one of the following spectrally compatible fluorophores: Alexa Fluor 546, Alexa Fluor 594, Alexa Fluor 647, IRDye 800CW, IRDye 680LT, or DY395XL (similar to Alexa Fluor 430) (Supplemental Table 3). After washing off excess secondary antibodies, sections were counterstained using 1 μg/mL DAPI (Thermo Fisher Scientific) for visualization of cell nuclei. Slides were then coverslipped using ImmuMount medium (Thermo Fisher Scientific) and imaged using a multichannel wide-field epifluorescence microscope (see below).

Image acquisition. Images were acquired from whole sections using the Axio Imager.Z2 slide scanning fluorescence microscope (Zeiss) equipped with a ×20/0.8 Plan-Apochromat (Phase-2) nonimmersion objective (Zeiss), a high resolution ORCA-Flash 4.0 sCMOS digital camera (Hamamatsu), a 200W X-Cite 200DC broad band lamp source (Excelitas Technologies), and 9 customized filter sets (Semrock) optimized to detect the following fluorophores: Alexa Fluor 546, Alexa Fluor 594, Alexa Fluor 647, IRDye 800CW, IRDye 680LT, or DY395XL. Image tiles (600 × 600 μm viewing area) were individually captured at 0.325 micron/pixel spatial resolution, and the tiles stitched into whole specimen images using the ZEN 2 image acquisition and analysis software program (Zeiss). Pseudocolored stitched images were overlaid in Imaris 9.2.1 (Bitplane) as individual layers to create multicolored merged composites.

Immunohistochemistry analysis. Each tissue sample was examined in Imaris 9.2.1 to quantify the number of CD3$^+$CD8$^+$ T cells per μm^2. Veins (SMA$^-$) and arteries (SMA$^+$) were chosen for each patient sample where possible (10 of each per sample). If a sample did not contain enough discernible arteries or veins, the remaining regions of interest (ROIs) were sampled irrespective of vessel type and grouped in the appropriate classification for analysis such that 20 vessels were quantified per sample. Total vessel area was calculated using the surfaces function in Imaris to

outline the cross-sectional area (μm²) of each vessel. The number of $CD3^+CD8^+$ T cells within the vessel surface (luminal) or outside the vessel surface (perivascular/abluminal) was quantified (Supplemental Table 4). $CD8^+$ T cells were scored as $DAPI^+$, $CD3^+$, and $CD8^+$ (Supplemental Figure 2). Cells were only counted as a $CD8^+$ T cell if they also costained with the $CD3^+$ T cell ontogeny marker. A variety of cells including monocytes and NK cells are $CD3^-CD8^+$, necessitating the use of both stains. For each vessel surface created in this analysis, the number of $IBA1^+CD68^+$ monocytes/macrophages per μm² was also quantified. These values were divided by the vessel area to generate the number of $IBA1^+CD68^+$ cells. All quantifications were made by 2 independent researchers blinded to the tissue classification and clinical data.

Confocal imaging of granzyme B. A representative CM^+ Seq^{hi} HIV^- serial section was stained with $CD8^+$ (Invitrogen, MA1-80231), granzyme B (Thermo Fisher Scientific, MA5-12469), and CD31 (Synaptic Systems, 351004) primary antibodies followed by staining with: Rhodamine Red X ($CD8^+$), Alexa Fluor 488 (granzyme B), and Alexa Fluor 647 (CD31) secondary antibodies (Supplemental Table 3). Sections were deparaffinized by washing twice for 3 minutes in xylene (Macron, 8668-16), then once for 3 minutes in 1:1 (vol/vol) xylene/100% ethanol. Sections were washed twice for 3 minutes in 100% ethanol, then once for 3 minutes each in graded 95%, 70%, and 50% ethanol. Sections were rehydrated by washing three times for 1 minute in dH_2O, then slides were placed in 10 mM Tris/EDTA Buffer (pH 9.0). Slides were microwaved for 10 minutes at 100% power, then cooled to room temperature for 30 minutes and washed three times for 1 minute in dH_2O. Slides were blocked using 1:20 True Black (Biotium, 23007 diluted in 70% EtOH) for 5 minutes, then washed three times for 1 minute in dH_2O and then 1:10 FcR Blocker + Background Buster (NB309 + NB306) for 15 minutes, then washed three times for 1 minute in dH_2O. Slides were incubated with primary antibodies for 45 minutes then washed. Slides were incubated with secondary antibodies for 45 minutes then washed. Finally, slides were dried and coverslipped. A second serial section from the same patient and location was stained with the same primary and secondary antibodies for CD8 and CD31 as well as only secondary antibodies for granzyme B to verify that the staining was specific. Fluorescent images were acquired using an Olympus FV1200 laser scanning confocal microscope equipped with 405, 488, 559, and 635 laser lines; 4 side window photomultiplier tubes for simultaneous 4 channel acquisition; and chromatic aberration corrected ×60/1.4 NA objective. Scans encompassing an area with $CD8^+$ T cells were imaged and then collected and analyzed using 9.2.1.

HIV analysis. Brain sections were analyzed for the presence of HIV p24 antigen using monoclonal mouse anti-HIV p24 (DAKO, M0857) with appropriate antibody controls. Analyses of sections from a patient with HIV encephalitis and a patient with atherosclerotic cardiovascular disease were included as positive and negative controls, respectively. HIV p24 retrieval was performed by steaming in Tris-EDTA buffer (pH 9.0) for 20 minutes. Peroxidase blocking was performed with dual enzyme block (DAKO), and protein blocking was performed using TBS with 0.5% (vol/vol) Triton-X and 2.5% (vol/vol) donkey serum. Monoclonal mouse anti-HIV p24 (DAKO, M0857) was diluted to 1:10 to blocking buffer and incubated overnight at room temperature. PowerVision anti-mouse-HRP (Leica Biosystems) was applied as a secondary antibody for 30 minutes at room temperature. DAB (Abcam) was used as a chromogen. Sections were counterstained with 10% hematoxylin (DAKO). Images were processed using a whole-slide scanner, Aperio (Leica Biosystems).

Statistics. For differential T cell analysis, volume-normalized T cell ($CD3^+CD8^+$) and monocyte/macrophage ($IBA1^+CD68^+$) "total" cell counts were organized in table form with 1 count per row and were sorted by clinical class, then by the individual from whom counts were collected. This table was then imported into R (http://cran.r-project.org) version 3.5.3 (Great Truth) and the counts were scaled by 10^4, pedestalled by 2, and $\log_2$ transformed. Transformed counts (T) were then mixed-effects modeled using the lmer() function (linear mixed effects model), using clinical class (C) as the fixed effect while treating the individual (I) as a random variable (T ~ C + (1|I), REML = TRUE). The lsmeans() function was then applied to this model and the output from this function passed as input into cld() function to obtain a least square (LS) mean transformed count value for each level of clinical class along with the standard error of the mean (SEM), degrees of freedom (df), and the lower and upper confidence levels (CL) for each level of clinical class. To visually compare the LS-mean counts across levels of clinical class, the ggplot() function was used to generate a dot plot that included error bars to describe the lower and upper CL (0.95) for each LS-mean count, respectively. To calculate and test the difference between LS-mean counts for each possible pairwise comparison of clinical classes, the difflsmeans() function (which calculates differences of least squares means and confidence intervals for the factors of a fixed part of mixed effects model of lmer object) was used (adjust = "tukey"). *P* values generated by this function were multiple comparison corrected (MCC) using the p.adjust() function (method = "FDR"). To avoid overfit conclusions, the entire procedure was repeated under bootstrap (leave-one-out) condition in 2 methods: (a) by removing 1 row count at a time, and (b) by removing all counts collected from 1 individual at a time. Comparisons of LS-mean counts between levels of clinical factors having an MCC FDR adjusted *P* less than 0.05 under the no-bootstrap condition, and both bootstrap conditions were deemed to have a significant difference in the number of total T cells or monocytes/macrophages. The entire procedure was repeated for abluminal and luminal counts separately. Finally, the entire procedure described was repeated yet again for each of the 3 starting tables of T cell counts using a modified clinical class coding that described the origin of counts, artery versus vein. Data were then imported into GraphPad Prism 8.0.1 to generate graphs.

Study approval. The study was approved by the IRBs of the University of Malawi College of Medicine, Blantyre, Malawi; Michigan State University, East Lansing, Michigan, USA; and the Brigham and Women's Hospital, Boston, Massachusetts, USA (47). Informed consent was obtained from a parent/guardian accompanying children admitted to the PRW at Queen Elizabeth Central Hospital (Blantyre, Malawi) at the time of admission.

Author contributions

BAR, MM, DM, LHM, DBM, and SKP conceptualized the experimental design, developed the antibody panel, and obtained funding for the study. TET and KBS conducted the parent study and provided invaluable insight on and access to the patient cohort and archived data. MM prepared the HBCC tissue blocks for mounting. BAR imaged the H&E sections. DM performed MP-IHC. OLAN analyzed the H&E sections and quantified the

percentage of vessels parasitized. MHL and AN performed p24 analysis. BAR and MM independently analyzed all MP-IHC images and performed all quantification. BAR, MM, DBM, and SKP conducted data interpretation. KRJ performed statistical analysis. BAR and SKP wrote the first draft of the manuscript. BAR and MM prepared all figures. BAR and MM had equal intellectual contribution and their order as co–first authors was determined by the amount of time they contributed. All authors revised the manuscript and gave final approval for publication.

Acknowledgments

This research was supported by the Intramural Research Program of the National Institute of Allergy and Infectious Diseases, Laboratory of Immunogenetics and the National Institute of Neurological Disorders and Stroke of the National Institutes of Health. We thank all the patients' guardians who generously donated tissue samples and acknowledge the support of the doctors and nurses across all trial sites.

Address correspondence to: Susan K. Pierce, Laboratory of Immunogenetics, NIAID, NIH, 5625 Fishers Lane, Room 4S-04, MSC 9418, Rockville, Maryland 20852, USA. Phone: 301.496.9589; Email: spierce@niaid.nih.gov. Or to: Dorian B. McGavern, NINDS, NIH, 10 Center Drive, Building 10, Room 5N240C, Bethesda, Maryland 20892, USA. Phone: 301.443.7949; Email: mcgavernd@ninds.nih.gov.

1. WHO. World Malaria Report. https://www.who.int/malaria/publications/world-malaria-report-2018/report/en/. Published November 2018. Accessed February 12, 2020.
2. WHO. Severe malaria. *Trop Med Int Health*. 2014;19(Suppl 1):7–131.
3. Mishra SK, Newton CR. Diagnosis and management of the neurological complications of falciparum malaria. *Nat Rev Neurol*. 2009;5(4):189–198.
4. Taylor TE, et al. Differentiating the pathologies of cerebral malaria by postmortem parasite counts. *Nat Med*. 2004;10(2):143–145.
5. Dunst J, Kamena F, Matuschewski K. Cytokines and chemokines in cerebral malaria pathogenesis. *Front Cell Infect Microbiol*. 2017;7:324.
6. Lyke KE, et al. Association of HLA alleles with Plasmodium falciparum severity in Malian children. *Tissue Antigens*. 2011;77(6):562–571.
7. Armah HB, et al. Cerebrospinal fluid and serum biomarkers of cerebral malaria mortality in Ghanaian children. *Malar J*. 2007;6:147.
8. McGuire W, Knight JC, Hill AV, Allsopp CE, Greenwood BM, Kwiatkowski D. Severe malarial anemia and cerebral malaria are associated with different tumor necrosis factor promoter alleles. *J Infect Dis*. 1999;179(1):287–290.
9. Koch O, et al. IFNGR1 gene promoter polymorphisms and susceptibility to cerebral malaria. *J Infect Dis*. 2002;185(11):1684–1687.
10. Newton CR, et al. Intracranial pressure in African children with cerebral malaria. *Lancet*. 1991;337(8741):573–576.
11. Brown H, et al. Evidence of blood-brain barrier dysfunction in human cerebral malaria. *Neuropathol Appl Neurobiol*. 1999;25(4):331–340.
12. Seydel KB, et al. Brain swelling and death in children with cerebral malaria. *N Engl J Med*. 2015;372(12):1126–1137.
13. Enwere G. A review of the quality of randomized clinical trials of adjunctive therapy for the treatment of cerebral malaria. *Trop Med Int Health*. 2005;10(11):1171–1175.
14. Warrell DA, et al. Dexamethasone proves deleterious in cerebral malaria. A double-blind trial in 100 comatose patients. *N Engl J Med*. 1982;306(6):313–319.
15. Hoffman SL, et al. High-dose dexamethasone in quinine-treated patients with cerebral malaria: a double-blind, placebo-controlled trial. *J Infect Dis*. 1988;158(2):325–331.
16. Taylor TE, Molyneux ME, Wirima JJ, Borgstein A, Goldring JD, Hommel M. Intravenous immunoglobulin in the treatment of paediatric cerebral malaria. *Clin Exp Immunol*. 1992;90(3):357–362.
17. van Hensbroek MB, et al. The effect of a monoclonal antibody to tumor necrosis factor on survival from childhood cerebral malaria. *J Infect Dis*. 1996;174(5):1091–1097.
18. Di Perri G, et al. Pentoxifylline as a supportive agent in the treatment of cerebral malaria in children. *J Infect Dis*. 1995;171(5):1317–1322.
19. Lell B, et al. Pentoxifylline as an adjunct therapy in children with cerebral malaria. *Malar J*. 2010;9:368.
20. Hawkes MT, et al. Inhaled nitric oxide as adjunctive therapy for severe malaria: a randomized controlled trial. *Malar J*. 2015;14:421.
21. Conroy AL, et al. Methemoglobin and nitric oxide therapy in Ugandan children hospitalized for febrile illness: results from a prospective cohort study and randomized double-blind placebo-controlled trial. *BMC Pediatr*. 2016;16(1):177.
22. Hemmer CJ, Kern P, Holst FG, Nawroth PP, Dietrich M. Neither heparin nor acetylsalicylic acid influence the clinical course in human Plasmodium falciparum malaria: a prospective randomized study. *Am J Trop Med Hyg*. 1991;45(5):608–612.
23. Namutangula B, Ndeezi G, Byarugaba JS, Tumwine JK. Mannitol as adjunct therapy for childhood cerebral malaria in Uganda: a randomized clinical trial. *Malar J*. 2007;6:138.
24. Newton CR, et al. Intracranial hypertension in Africans with cerebral malaria. *Arch Dis Child*. 1997;76(3):219–226.
25. Mohanty S, et al. Brain swelling and mannitol therapy in adult cerebral malaria: a randomized trial. *Clin Infect Dis*. 2011;53(4):349–355.
26. Maitland K, et al. Randomized trial of volume expansion with albumin or saline in children with severe malaria: preliminary evidence of albumin benefit. *Clin Infect Dis*. 2005;40(4):538–545.
27. Akech S, et al. Volume expansion with albumin compared to gelofusine in children with severe malaria: results of a controlled trial. *PLoS Clin Trials*. 2006;1(5):e21.
28. White NJ, Turner GD, Medana IM, Dondorp AM, Day NP. The murine cerebral malaria phenomenon. *Trends Parasitol*. 2010;26(1):11–15.
29. Swanson PA, et al. CD8+ T cells induce fatal brainstem pathology during cerebral malaria via luminal antigen-specific engagement of brain vasculature. *PLoS Pathog*. 2016;12(12):e1006022.
30. Penet MF, et al. Imaging experimental cerebral malaria in vivo: significant role of ischemic brain edema. *J Neurosci*. 2005;25(32):7352–7358.
31. Hoffmann A, et al. Experimental cerebral malaria spreads along the rostral migratory stream. *PLoS Pathog*. 2016;12(3):e1005470.
32. Riggle BA, et al. MRI demonstrates glutamine antagonist-mediated reversal of cerebral malaria pathology in mice. *Proc Natl Acad Sci U S A*. 2018;115(51):E12024–E12033.
33. Potchen MJ, et al. 1.5 Tesla magnetic resonance imaging to investigate potential etiologies of brain swelling in pediatric cerebral malaria. *Am J Trop Med Hyg*. 2018;98(2):497–504.
34. Howland SW, et al. Brain microvessel cross-presentation is a hallmark of experimental cerebral malaria. *EMBO Mol Med*. 2013;5(7):984–999.
35. Howland SW, Poh CM, Rénia L. Activated brain endothelial cells cross-present malaria antigen. *PLoS Pathog*. 2015;11(6):e1004963.
36. Dorovini-Zis K, et al. The neuropathology of fatal cerebral malaria in malawian children. *Am J Pathol*. 2011;178(5):2146–2158.
37. Barrera V, et al. Comparison of $CD8^+$ T cell accumulation in the brain during human and murine cerebral malaria. *Front Immunol*. 2019;10:1747.
38. Hochman SE, et al. Fatal pediatric cerebral malaria is associated with intravascular monocytes and platelets that are increased with HIV coinfection. *mBio*. 2015;6(5):e01390–e01315.
39. Frevert U, Nacer A. Fatal cerebral malaria: a venous efflux problem. *Front Cell Infect Microbiol*. 2014;4:155.
40. Milner DA, et al. Supraorbital postmortem brain sampling for definitive quantitative confirmation of cerebral sequestration of Plasmodium falciparum parasites. *J Infect Dis*. 2012;205(10):1601–1606.
41. Shaw TN, et al. Perivascular arrest of CD8+ T cells is a signature of experimental cerebral malaria. *PLoS Pathog*. 2015;11(11):e1005210.
42. Haque A, et al. Granzyme B expression by CD8+ T cells is required for the development of experimental cerebral malaria. *J Immunol*. 2011;186(11):6148–6156.
43. Gordon EB, et al. Targeting glutamine metabolism rescues mice from late-stage cerebral malaria. *Proc Natl Acad Sci U S A*. 2015;112(42):13075–13080.

44. Grau GE, et al. Late administration of monoclonal antibody to leukocyte function-antigen 1 abrogates incipient murine cerebral malaria. *Eur J Immunol*. 1991;21(9):2265–2267.
45. Bronzan RN, et al. Bacteremia in Malawian children with severe malaria: prevalence, etiology, HIV coinfection, and outcome. *J Infect Dis*. 2007;195(6):895–904.
46. Milner DA, et al. Quantitative assessment of multiorgan sequestration of parasites in fatal pediatric cerebral malaria. *J Infect Dis*. 2015;212(8):1317–1321.
47. Taylor TE, et al. Differentiating the pathologies of cerebral malaria by postmortem parasite counts. *Nat Med*. 2004;10(2):143–145.